2018-01-0123 Published 03 Apr 2018

The Synthetic 3DOF Wheel Force for Passenger Vehicle Based on Predicted Frequency Response Function Model

Shengjie Xu CATARC

Citation: Xu, S., "The Synthetic 3DOF Wheel Force for Passenger Vehicle Based on Predicted Frequency Response Function Model," SAE Technical Paper 2018-01-0123, 2018, doi:10.4271/2018-01-0123.

Abstract

To determine the vehicle chassis requirements, wheel force transducer (WFT) have been the best option when it is being used in targeting customer correlation or determining the effective use of the proving ground. However, using wheel force transducer in customer correlation fleet test is often unfeasible due to the huge cost and low practicability. As a result, engineers have to choose other transducer measures. This paper describes an effective approach of wheel force prediction by using the frequency response function (FRF) model of vehicle dynamic system.

A vehicle system linear modelling technique is used. For the system identification of FRF, the acceleration and wheel force time history data, as system input and output, are collected from an instrumented passenger car as it traverses in different real-world proving ground surfaces. The obtained FRF represents the complex suspension mechanical model. Once the FRF is calculated, the predicted force signal can be implemented.

The quality evaluation of prognostication results is made by comparing the synthetic and real-world wheel force signals in time/frequency domain and frequency-related pseudo damage. The result indicates that the FRF derived from real-world data is an effective modelling tool. Furthermore, it is a promising application in the field of customer usage fleet test and suspension dynamic system modelling or control.

Introduction

Wheel force transducer has been widely proven in the modern development process of the worldwide automotive industry as the most effective approach for the vehicle spindle dynamic force acquisition. The accurate input load benefits the FEA engineer in suspension, body/frame durability evaluation [1, 2, 3, 4].

However, the implement of a WFT-involved road test is undoubtedly a time-consuming process, which means if the engineer needs strong confidence about the collected data one should consider the unsprung mass deviation, wheel balancing, and measurement plane in practical engineering [5, 6]. In addition, the design, calibration and manufacturing process make the WFT a relatively high price [7, 8]. Due to these reasons, the sensor is suitable for accurate road load data acquisition (RLDA) in proving ground instead of massive application in public road load data acquisition. When the engineering problem presents on our test planner's desktop, the application of wheel force transducer in fleet test level is definitely not a rational option. It is beneficial to develop a force prediction tool as a substitution of wheel force transducer in an acceptable accuracy and price [9].

In the field of customer correlation, wheel axle load is treated as primary correlation factor in the process of mathematical optimization. The common engineering techniques are David's Integrated Durability Engineering, Dressler's Reference-Customer-Spectrum and Andrew's Relative Damage Spectrum [10, 11, 12]. In the field of dynamic force reconstruction, Dobson discussed the theoretical technique used in the calculation of excitation force [13], however it states that the disadvantage of frequency domain model had prediction problems in the region of anti-resonances. In the work of Cornelis, it suggests a force prediction technique which is Augmented Kalman Filter virtual sensing [14]. The deficiency of their current work is that only constant frequency sinusoidal input forces were being discussed and the prediction is a simulation in numerical environment.

This paper will explore the feasibility study of the FRF modelling method in durability and reliability. We first give a brief description of our prediction model architecture, then describe the creation of the modelling datasets and the data pre-processing. We conclude by summarizing the results obtained in the prediction model.

Technique Background

For most experimental modal analysis, the impact force ordinarily acts as inputs and acceleration acts as outputs [15]. However, in our case, to build a force prediction model, we treat the wheel center acceleration as inputs and wheel force as outputs. To prove the feasibility of such hypothesis, an argument is made in the following passage. As a quarter car

FIGURE 1 Vertical oscillation model of quarter car suspension.

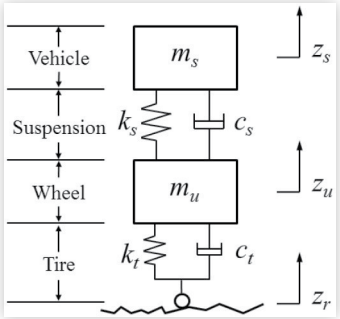

system is shown in Figure 1, where transfer function derivation of the vertical suspension system is made.

The second-order differential equations of the oscillation model can be derived by:

$$m_s\ddot{z}_s + c_s\dot{z}_s + k_s z_s = c_s\dot{z}_u + k_s z_u \tag{1}$$

$$m_u\ddot{z}_u + c_s\dot{z}_u + k_s z_u + c_t\dot{z}_u + k_t z_u = c_s\dot{z}_s + \cdots + k_s z_s + c_t\dot{z}_r + k_t\, z_r \ldots \tag{2}$$

$$c_t\dot{z}_u + k_t z_u - f_z = c_t\dot{z}_r + k_t z_r \tag{3}$$

where:

m_s Sprung mass

m_u Unsprung mass

k_s Vertical stiffness coefficient of the suspension

k_t Vertical stiffness coefficient of the tire

c_s Vertical damping coefficient of the suspension

c_t Vertical damping coefficient of the tire

z_s Vertical displacement of the sprung mass

z_u Vertical displacement of the unsprung mass

z_r Vertical road displacement

f_z Vertical force of wheel center

Apply Fourier transformation to equation (1) (2) (3), we obtained:

$$\left(m_s + c_s\frac{1}{i\omega} - k_s\frac{1}{\omega^2}\right)\ddot{Z}_s = \left(c_s\frac{1}{i\omega} - k_s\frac{1}{\omega^2}\right)\ddot{Z}_u \tag{4}$$

$$\left(m_u + c_s\frac{1}{i\omega} - k_s\frac{1}{\omega^2} + c_t\frac{1}{i\omega} - k_t\frac{1}{\omega^2}\right)\ddot{Z}_u = \ldots \left(c_s\frac{1}{i\omega} - k_s\frac{1}{\omega^2}\right)\ddot{Z}_s + \left(c_t\frac{1}{i\omega} - k_t\frac{1}{\omega^2}\right)\ddot{Z}_{rz} \tag{5}$$

$$\left(c_t\frac{1}{i\omega} - k_t\frac{1}{\omega^2}\right)\ddot{Z}_u - F_z = \left(c_t\frac{1}{i\omega} - k_t\frac{1}{\omega^2}\right)\ddot{Z}_r \tag{6}$$

Where:

Z_s Fourier transformation of vertical displacement of the sprung mass

Z_u Fourier transformation of vertical displacement of the unsprung mass

Z_r Fourier transformation of vertical road displacement

F_z Fourier transformation of vertical force of wheel center

ω Angular frequency

The transfer function $H(\omega)$ of spindle acceleration $\ddot{Z}_u$ and input force F_z is defined as:

$$H(\omega) = \frac{F_z}{\ddot{Z}_u} \tag{7}$$

$$H(\omega) = \frac{1}{i\omega^2}\left[\frac{(c_s\omega - k_s i)^2}{m_s i\omega^2 + c_s\omega - k_s i} - \left(m_u i\omega^2 + c_s\omega - k_s i\right)\right] \tag{8}$$

The above derivation reveals that the amplitude of the FRF between spindle acceleration and wheel force is a function of angular frequency. The dynamic force is, given constant coefficient for stiffness and damping factor, proportional to input acceleration in each angular frequency.

However, in real world, the appearance of nonlinearity will arise when the coil spring being compressed to the bottom position. Further, According to Barber's research [16], the natural 'Force-Velocity' curve of damper should be shaped like a hysteresis 'backbone' due to its nonlinearity and memory characteristic. In 'White Box' modelling or spatial model, the expression of 3DOF model needs to be built, which means the strong non-linearity relation between force and acceleration in longitudinal and lateral need to be developed [13]. In FRF modelling, the FRF matrices will be built by one calculation process and meanwhile it remains the nonlinearity information by frequency-dependent gain.

To date, the direct measurement of the spatial properties from experimental frequency response data has been limited to relatively simple systems. In vehicle system, considering the difficulty of building a precise tire model in longitudinal and lateral, the spatial modelling of longitudinal and lateral system is not being discussed in this paper [17].

Predicted FRF Model

The architecture of the prediction model is illustrated in Figure 2. First, the input and output parameters of the prediction model have been proven as a valid mathematical relationship by a mechanical system analysis in the previous discussion. Then, the RLDA of the target vehicle is implemented to obtain the excitation data of the wheel-tire system. A subsequent signal pre-processing is applied to the raw data. With the input and output data, a FRF fast estimation is calculated. Once the FRF is valid for a good model, a following convolution and inverse Fast Fourier Transform can be applied to the input signal.

Input/Output and FRFs

The suspension system of one vehicle corner was considered as a 3DOF system with acceleration as inputs and wheel force

FIGURE 2 Architecture of the prediction model.

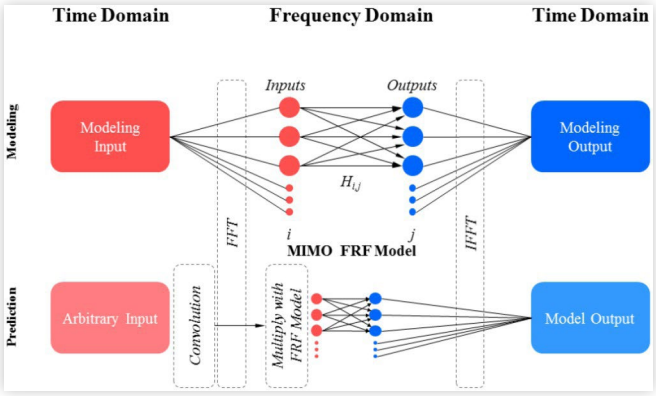

FIGURE 3 The FRF matrices of the prediction model.

Input \ Output	y_1 LF Fx	y_2 LF Fy	y_3 LF Fz	y_4 RF Fx	y_5 RF Fy	y_6 RF Fz	y_7 LR Fx	y_8 LR Fy	y_9 LR Fz	y_{10} RR Fx	y_{11} RR Fy	y_{12} RR Fz
x_1 LF Ax	$H_{1,1}$	$H_{1,2}$	$H_{1,3}$	$H_{1,4}$	$H_{1,5}$	$H_{1,6}$	$H_{1,7}$	$H_{1,8}$	$H_{1,9}$	$H_{1,10}$	$H_{1,11}$	$H_{1,12}$
x_2 LF Ay	$H_{2,1}$	$H_{2,2}$	$H_{2,3}$	$H_{2,4}$	$H_{2,5}$	$H_{2,6}$	$H_{2,7}$	$H_{2,8}$	$H_{2,9}$	$H_{2,10}$	$H_{2,11}$	$H_{2,12}$
x_3 LF Az	$H_{3,1}$	$H_{3,2}$	$H_{3,3}$	$H_{3,4}$	$H_{3,5}$	$H_{3,6}$	$H_{3,7}$	$H_{3,8}$	$H_{3,9}$	$H_{3,10}$	$H_{3,11}$	$H_{3,12}$
x_4 RF Ax	$H_{4,1}$	$H_{4,2}$	$H_{4,3}$	$H_{4,4}$	$H_{4,5}$	$H_{4,6}$	$H_{4,7}$	$H_{4,8}$	$H_{4,9}$	$H_{4,10}$	$H_{4,11}$	$H_{4,12}$
x_5 RF Ay	$H_{5,1}$	$H_{5,2}$	$H_{5,3}$	$H_{5,4}$	$H_{5,5}$	$H_{5,6}$	$H_{5,7}$	$H_{5,8}$	$H_{5,9}$	$H_{5,10}$	$H_{5,11}$	$H_{5,12}$
x_6 RF Az	$H_{6,1}$	$H_{6,2}$	$H_{6,3}$	$H_{6,4}$	$H_{6,5}$	$H_{6,6}$	$H_{6,7}$	$H_{6,8}$	$H_{6,9}$	$H_{6,10}$	$H_{6,11}$	$H_{6,12}$
x_7 LR Ax	$H_{7,1}$	$H_{7,2}$	$H_{7,3}$	$H_{7,4}$	$H_{7,5}$	$H_{7,6}$	$H_{7,7}$	$H_{7,8}$	$H_{7,9}$	$H_{7,10}$	$H_{7,11}$	$H_{7,12}$
x_8 LR Ay	$H_{8,1}$	$H_{8,2}$	$H_{8,3}$	$H_{8,4}$	$H_{8,5}$	$H_{8,6}$	$H_{8,7}$	$H_{8,8}$	$H_{8,9}$	$H_{8,10}$	$H_{8,11}$	$H_{8,12}$
x_9 LR Az	$H_{9,1}$	$H_{9,2}$	$H_{9,3}$	$H_{9,4}$	$H_{9,5}$	$H_{9,6}$	$H_{9,7}$	$H_{9,8}$	$H_{9,9}$	$H_{9,10}$	$H_{9,11}$	$H_{9,12}$
x_{10} RR Ax	$H_{10,1}$	$H_{10,2}$	$H_{10,3}$	$H_{10,4}$	$H_{10,5}$	$H_{10,6}$	$H_{10,7}$	$H_{10,8}$	$H_{10,9}$	$H_{10,10}$	$H_{10,11}$	$H_{10,12}$
x_{11} RR Ay	$H_{11,1}$	$H_{11,2}$	$H_{11,3}$	$H_{11,4}$	$H_{11,5}$	$H_{11,6}$	$H_{11,7}$	$H_{11,8}$	$H_{11,9}$	$H_{11,10}$	$H_{11,11}$	$H_{11,12}$
x_{12} RR Az	$H_{12,1}$	$H_{12,2}$	$H_{12,3}$	$H_{12,4}$	$H_{12,5}$	$H_{12,6}$	$H_{12,7}$	$H_{12,8}$	$H_{12,9}$	$H_{12,10}$	$H_{12,11}$	$H_{12,12}$

as outputs. Consequently, as shown in Figure 3, the matrices [M] of the transfer function contain 12x12 FRFs, which means each FRF consist of the overall gain information in each frequency line. One should notice that the acquired FRF is an approximation linear model to describe the frequency model of the vehicle suspension system.

Convolution and Inverse FFT

The convolution is the process that determines the system output. As convolution in time domain is the same as multiplication in frequency domain, the FRF and the input acceleration are multiplied together in frequency domain. The above time/frequency domain conversion is achieved by FFT.

The strength of FRF multiplication is that it ignores the construction of physical system. Still, it contains the dynamic information of all three degree of freedom. Besides, the algorithm is represented by a straightforward arithmetic operation which can be solved by direct calculation. Due to its high-speed computational characteristic, the FFT algorithm is suitable for vehicle force on-board monitoring [18]. The following step is changing the prediction data back into time domain via Inverse Fast Fourier Transformation (IFFT) to obtain prediction force.

Experiment

Road Load Data Acquisition

The measurement data was recorded in 512 Hz sample rate at two proving grounds with one well-instrumented passenger car. The test vehicle has a GVW in 1421 kg, front suspension is McPherson and rear suspension is twist beam.

Tri-axis accelerometers were positioned on the spindle of all four wheels. Dynamic wheel force was recorded through a wheel force transducer assembled with a modified wheel rim. The transducers mentioned above is shown in Figure 4. In RLDA, compared to a normal modal analysis test, wheel force transducer acts as a force gauge impact hammer and the role of accelerometer is unchanged.

As shown in Table 1, the RLDA was taken under specific durability procedure in each proving ground. The overall test track has 45 events. It is encouraging to collect the load under every possible road events for the purpose of covering enough spatial properties of the test vehicle [13]. Normally, the nonlinear part in a vehicle is the elastic part, such as shock absorber, bushing and jounce bumper [19]. The diverse road events covered in our experiment range from low-frequency driving manoeuvre to road induced high-frequency vibration [11].

FIGURE 4 Wheel force transducer and accelerometer were mounted on an instrumented test vehicle.

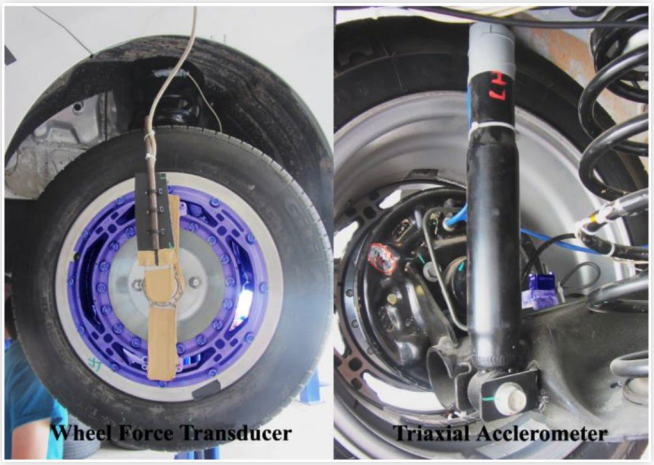

TABLE 1 Test track and dataset information.

Dataset	PG	Files	Track Description	Length (sec)
Modelling	PG 1	A	Durability Procedure Track1	416
		B	Durability Procedure Track2	1136
		C	Braking	356
		D	Longwave and Twist	244
		E	Powertrain	600
	PG 2	J01	Durability Procedure	800
		J02	Figure 8 and Braking	520

FIGURE 5 The combined data of channel left front longitudinal, where red curve is input acceleration and blue curve is output wheel force.

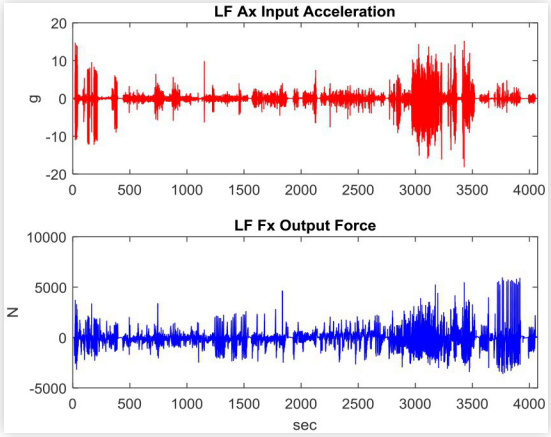

Data Pre-Processing

The acquired data was recorded as eight separated data files. Merge all the data in modelling set into a combined dataset which have 4072 seconds in length; an example of combined data is shown in Figure 5. Remove mean value for each channel. Subsequently, split the combined data set into acceleration data (inputs) and wheel force data (outputs) for FRF modelling.

Results

Coherence and FRF Analysis To assess the noise level and the accuracy of the transfer function measurements, an ordinary coherence of is performed. The ordinary coherence can be stated as the product of transfer function and its inverse function. As such, it indicates the quality of reflection through the system. If a system is linear and none of our measurements is contaminated by noise, the reflection is perfect and we get back everything we put in. The corresponding Coherence will be exactly 1. If a system is non-linear or if extraneous noise has been interjected at the input or output, the reflection will be less efficient and the coherence will be less than one.

The ordinary coherence of the experimental system is shown in Figure 6. We conclude that the transfer function system we defined shows very good linearity and noise-free in vertical, w.

Hereas it shows noisy and non-linearity in longitudinal and lateral. In further explanation:

- Longitudinal coherence of front wheels indicate that it has good linearity in most frequency except the frequency band between 3-10 Hz and around 25 Hz.
- Longitudinal coherence of rear wheels indicate that it has good linearity in most frequency except the frequency band between 1-8 Hz and around 12 Hz.
- Lateral coherence of front wheels indicate that it has poor linearity in the frequency **band** between 5-20 Hz and 50-75 Hz

FIGURE 6 The 3DOF coherence of the vehicle suspension system.

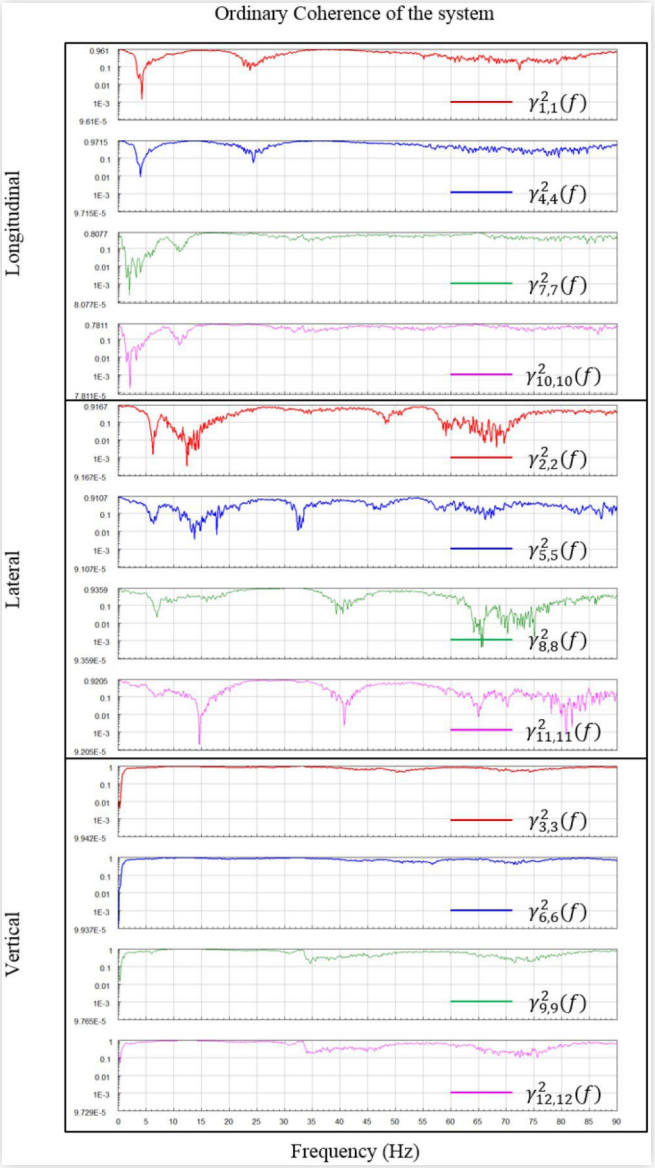

- Lateral coherence of rear wheels indicate that it has poor linearity in the frequency band between 10-20 Hz, 30-45 Hz and 60-85 Hz

It indicates a problem within the FRF when the coherence is close to 0 at a certain frequency. Typically, the coherence at 2 Hz in longitudinal rear wheels and 15 Hz in lateral rear wheels is lower than 0.001. In such regions, the prediction force may leading invalid result [13].

The diagonal elements of the FRF matrices is illustrated in Figure 7. It shows rich information of the resonance and anti-resonance identification of the system to engineers. We conclude that significant damping exist in longitudinal and lateral FRF, whereas the vertical FRF has very small damping.

Prediction Result in Time Domain Time history comparison is the most significant indicator of the force

prediction quality. The overall combined time history prediction result is shown in Figure 8. Intuitively, the error band of all three directions is similar, longitudinal and lateral predicted force is not as perfect as the vertical. We pick out 15 road events distributed in different frequency for demonstration.

As an indicator for regression analysis, the root mean square error (RMSE) is introduced here. The RMSE is defined as the RMS of the error between target and achieved prediction data divided by the RMS of the target data, the resulting number was represented in percentage. When the target and predicted data converge, the error percentage should tend to 0% [20].

The calculated RMSE for each road event and rubric is listed in Table 2. The events were sorted in dominant frequency since each road event has a different dominant frequency. The corresponding RMSE was calculated under two types of signals which is unfiltered data and 1 Hz high-pass filtered data. For instance, for the event whose prominent frequency locates lower than 1 Hz, such as low-frequency driving manoeuvres: steering, braking and twist, the RMSE of unfiltered data was taken into account. On contrary, for the event whose dominant frequency is excited by road induced higher frequency, the RMSE of high-pass filtered data was counted.

In practical engineering, according to the road simulation test technical background of the author, the acceptable RMSE level of the drive file generation in road simulation test should fall into a range of 5-25% for the reason of the capability of the 6DOF road simulator is limited [20]. Still, it is a good durability test for those engineers who can converge the response signal to 25% RMSE in the process of full-vehicle road simulation. Hence, the acceptance criteria of the force prediction can be set to 25%.

Statistically, the averaged RMSE of the overall data is 39.8% in longitudinal, 54.6% in lateral, 27.1% in vertical. Moreover, as the RMSE distribution colour map shown in Figure 9, it indicates that the prediction signal generally follows the target signal in an acceptable level. As Table 2 reveals, the RMSE of vertical in low-frequency events mainly reaches into perfect interval. The rear longitudinal prediction force is bad since the target driving force of a FWD vehicle's rear wheel, as a denominator in RMSE, is relatively small. For higher frequency events, the predominantly trend is: longitudinal prediction distributed from great to bad; lateral

FIGURE 7 The diagonal elements of the 12 x 12 FRF matrices.

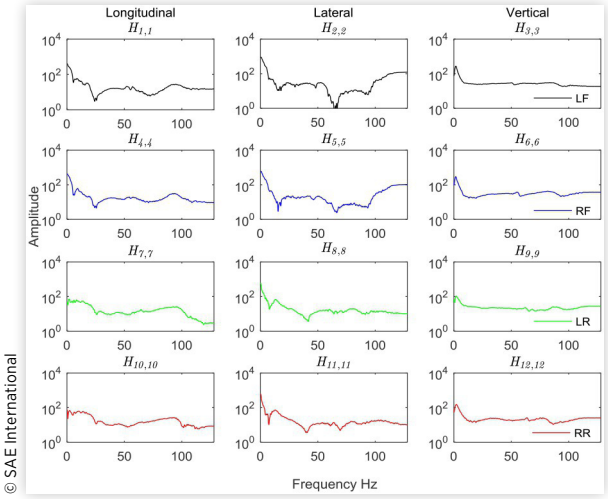

FIGURE 8 The time history comparison of the overall 3DOF force signal prediction.

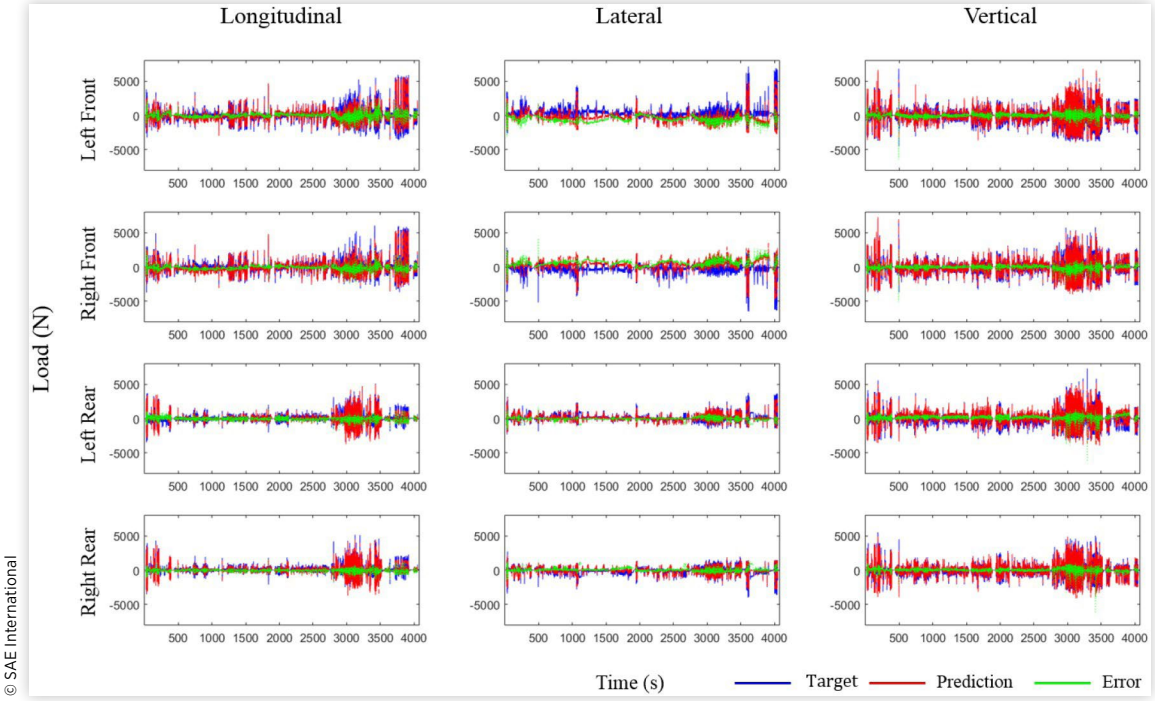

TABLE 2 RMSE of 3DOF force signal prediction and rubric table.

No.	Road Event	Dominant Frequency	Dominant Direction	Ch1 LF Fx	Ch2 LF Fy	Ch3 LF Fz	Ch4 RF Fx	Ch5 RF Fy	Ch6 RF Fz	Ch7 LR Fx	Ch8 LR Fy	Ch9 LR Fz	Ch10 RR Fx	Ch11 RR Fy	Ch12 RR Fz
1	Driveway	0.5 Hz	Vertical	38.1%	64.4%	23.3%	25.9%	68.5%	19.3%	94.6%	58.0%	33.7%	86.9%	57.2%	24.6%
2	Slalom Cobblestone	0.5 Hz	Lateral	59.9%	42.3%	35.1%	55.1%	49.0%	31.0%	30.8%	44.5%	32.4%	29.2%	44.0%	25.2%
3	City Brake	0.5 Hz	Longitudinal	20.7%	27.8%	22.5%	14.1%	35.5%	24.0%	80.2%	28.7%	44.8%	59.5%	27.6%	23.1%
4	Figure 8	0.5 Hz	All	27.0%	12.8%	10.1%	30.8%	14.4%	8.4%	160.1%	9.1%	13.9%	209.3%	10.7%	13.4%
5	Twist	0.5 Hz	Vertical	30.7%	67.4%	18.3%	25.6%	69.2%	16.3%	59.6%	85.8%	18.1%	52.0%	82.7%	18.0%
6	Manhole cover	2 Hz	Vertical	26.9%	38.0%	22.2%	29.7%	40.7%	27.4%	46.7%	43.2%	16.7%	47.3%	38.9%	20.7%
7	Variant Wave	8.5 Hz	Vertical	27.5%	34.5%	24.8%	24.2%	20.1%	26.6%	88.7%	32.5%	25.4%	50.3%	42.7%	22.8%
8	Railway Cross	9.5 Hz	Vertical	37.3%	65.3%	25.9%	32.1%	67.9%	29.6%	30.8%	32.0%	28.2%	18.8%	52.4%	22.6%
9	Belgian 1	10 Hz	All	48.2%	42.8%	22.3%	175.7%	53.4%	22.8%	20.8%	37.2%	18.9%	20.6%	42.3%	20.5%
10	Impact	10.5 Hz	Vertical	38.1%	51.6%	15.0%	30.0%	51.0%	13.6%	25.8%	27.7%	16.4%	19.5%	32.7%	18.1%
11	Cobblestone	10.5 Hz	All	54.7%	295.3%	23.2%	46.2%	272.3%	26.8%	29.2%	36.4%	23.3%	30.4%	35.8%	27.1%
12	Resonance	11 Hz	Vertical	39.9%	54.7%	13.2%	28.4%	54.0%	10.8%	30.5%	31.0%	17.0%	16.8%	36.1%	11.8%
13	Belgian 2	11 Hz	All	38.2%	57.6%	26.5%	65.2%	103.3%	24.0%	21.7%	73.1%	17.0%	24.4%	53.8%	20.9%
14	High way	18.5 Hz	All	98.5%	191.4%	49.4%	81.2%	278.8%	42.6%	46.2%	30.1%	25.0%	62.9%	79.4%	30.3%
15	Washboard	33 Hz	Vertical	64.3%	146.8%	15.1%	27.0%	246.2%	20.5%	11.6%	30.6%	15.4%	11.1%	31.2%	14.6%
RMSE				0-25%	25%-50%		50%-75%		75%-100%			>100%			
Level				Perfect	Great		Good		Bad			Not qualified			
The fitting of time history waveform				Time history waveform perfectly covered in both amplitude and phase.	Time history covers most signal well. However, minor peak amplitude and phase error happened due to the lack of sufficient prediction in minor regions.		Time history covers a qualified wave shape. The major error from minor drift or offset, amplitude and phase delay error can be found in minor regions.		Time history covers an undesirable shape. The major error from obvious drift offset or lack of sufficient amplitude in all x-axis. Another appearance is the error band is nearly similar to the amplitude of target signal.			Time history covers a terrible shape. However, the major error comes from low-frequency drift but not high-frequency oscillation. Another appearance is the error band is the error band is nearly similar to the amplitude of target signal.			
Counts (Appearance Probability)				59 (33%)	75 (42%)		27 (15%)		9 (5%)			10 (6%)			

FIGURE 9 RMSE distribution colour map of prediction result.

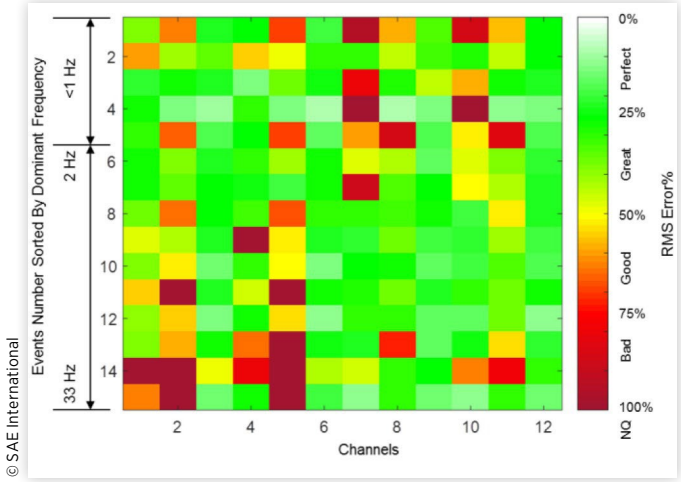

FIGURE 10 LF Fx ASD comparison of the target, response and error with FRF.

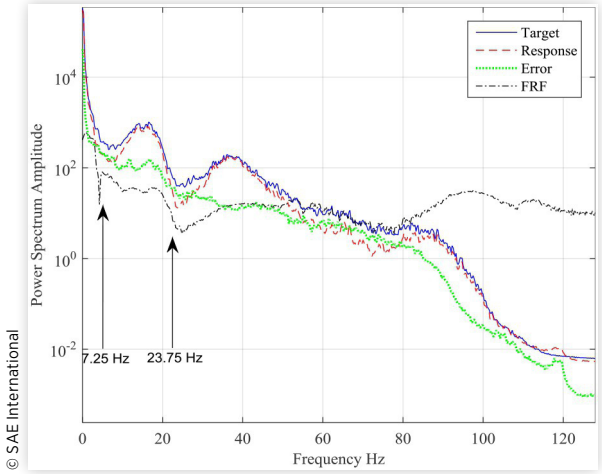

FIGURE 11 LF Fy ASD comparison of the target, response and error with FRF.

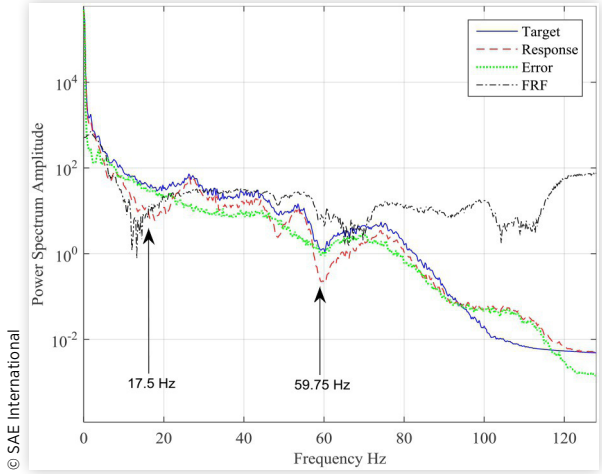

FIGURE 12 LF Fz ASD comparison of the target, response and error with FRF.

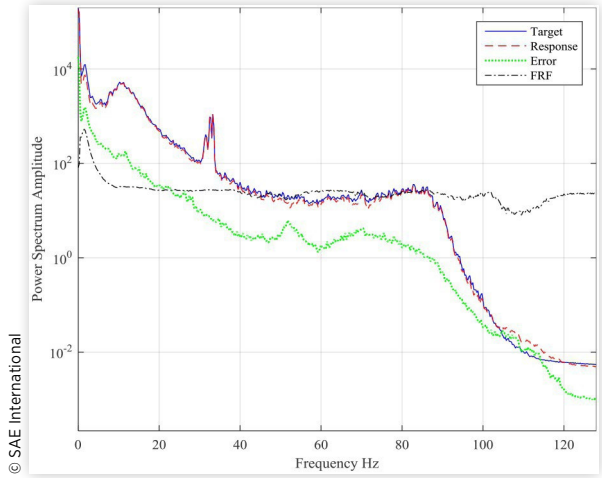

prediction of rear axle is perfect for most cases, however the lateral prediction of front wheel remains low accuracy. As Figure 8 reveals, it has too much drifting in the prediction of front suspension lateral.

In conclusion, only the prediction of vertical force shows a perfect and satisfied result.

Prediction Result in Frequency Domain The auto spectral density (ASD) is calculated for overall target/prediction force and the error signal. Overlay the ASD with the FRF of left front wheel, as Figure 10-12 shows, one can easily found that the error contents of the left front wheel locates at a specific frequency band where the FRF has strong noisy gain and nonlinearity. In particular, a significant error occurred at the central frequency of 7.25 Hz and 23.75 Hz for longitudinal and 17.5 Hz and 59.75 Hz for longitudinal with a 15 Hz bandwidth. Associated with the discussion in coherence section, we can conclude that the bad prediction result and low coherence located at the same non-linearity region due to the anti-resonance of the system. For the system with low anti-resonance, as the vertical system in Figure 12, the FRF modeling leads to a good prediction quality.

Prediction Result in Pseudo Damage In the field of durability optimization, wheel force is the primary target signal for damage evaluation in customer correlation or proving ground correlation. The reason is that WFT, as in load path, connects the road surface profile and the vehicle loads. Several common damage analysis techniques, such as level crossing and rainflow, are usually inclined to use WFT for calculation. Therefore, the primary preferable signal to be collected in customer usage pattern fleet test is WFT [10,12].

The purpose of this section is to investigate the feasibility of using FRF prediction force in customer correlation. Under a certain predefined pseudo S-N curve, as Table 3 shows, the pseudo damage is calculated for the overall prediction and target force. According to Andrew's conclusion, a 'Good' convergence of fatigue damage prediction is drop in a 0.5-2 interval of Prediction/ Target factor [12], since the 'log' arithmetic in damage calculation formula always magnify the

TABLE 3 The pseudo damage comparison of the overall prediction and target force.

Ch.	Channel Name	Target Damage	Prediction Damage	Prediction/ Target
1	LF Fx	2.78E + 17	1.59E + 17	57%
2	LF Fy	8.04E + 16	4.18E + 16	52%
3	LF Fz	1.37E + 18	1.28E + 18	93%
4	RF Fx	2.29E + 17	1.59E + 17	69%
5	RF Fy	6.24E + 16	3.37E + 16	54%
6	RF Fz	1.12E + 18	1.04E + 18	93%
7	LR Fx	2.80E + 17	2.78E + 17	99%
8	LR Fy	3.32E + 16	2.38E + 16	72%
9	LR Fz	1.02E + 18	9.62E + 17	94%
10	RR Fx	2.83E + 17	2.75E + 17	97%
11	RR Fy	3.65E + 16	2.57E + 16	70%
12	RR Fz	8.29E + 17	8.10E + 17	98%

damage value in ten times bigger. As Table 3 reveals that the vertical and rear longitudinal prediction force shows a perfect pseudo damage correlation. The prediction signal retains original damage up to 90% in vertical. On the other hand, the percentage of front longitudinal and lateral ranges from 50% to 70%. It reveals that the prediction signal has a good damage correlation in longitudinal and lateral.

According to Andrew's research, the frequency-dependent damage distribution is crucial when conducting damage comparison, the reason is each component has a specific resonance frequency, in other words, a 'fatigue sensitivity'. Consequently, in order to show the damage distribution of FRF prediction in frequency, a related damage spectrum (RDS) histogram is generated under a same pseudo S-N curve in pseudo damage calculation [12].

The bins of x-axis in RDS histogram represent the twelve channels' sixty frequency bands. For each channel, it has five bands sorted from low to high (0-2.2, 1.8-4.4, 3.6-8.8, 7.2-17.6 and 14.4-32 Hz). As the RDS histogram shown in Figure 11,

FIGURE 13 RDS of unfiltered overall RDS of prediction and target force.

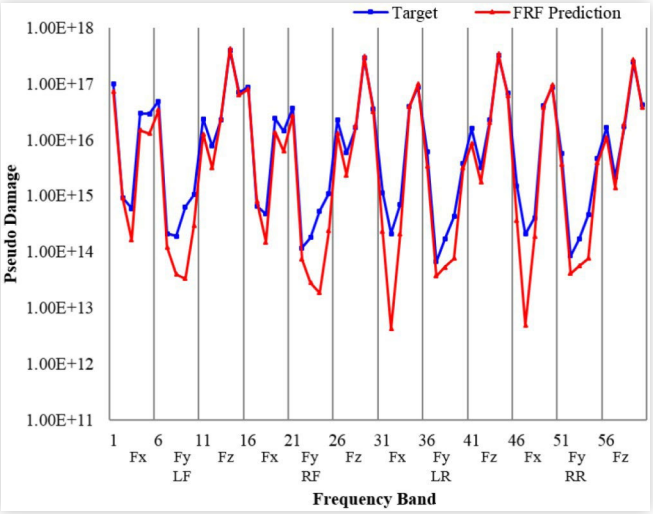

the frequency distributed damage of FRF prediction force cover most area of target force; in lateral, rear longitudinal channels the prediction force is lack of damage in medium or higher frequency band, which is unified with the conclusion in previous section.

The RDS result in Figure 13 reveals that the FRF predicted force in vertical and longitudinal has an ideal frequency distributed damage correlation which gives strong confidence of the application in customer correlation.

Conclusions and Outlook

This paper introduced a FRF based force prognostication algorithm The results and analysis shown in this paper suggests that this method is effective when applied in vertical direction for customer correlation fleet test or proving ground optimization. A theoretical transfer function formula has been introduced, which proves that it's feasible to bridge a frequency dependent numerical relationship for acceleration and dynamic force by FRF modelling. In order to generate FRFs for target vehicle, measured time history data is collected for multiple track surfaces in proving ground. Prediction force is prognosticated by the convolution of input signal and FRFs. The result evaluation is executed and it proves that, in time domain and damage, the algorithm shows an good prediction accuracy in vertical and an acceptable accuracy in longitudinal. The discussion about coherence and frequency domain indicates that the error contents accompany with where the FRF noisy/nonlinearity pattern happens.

The paper suggests that the predicted frequency response function model is valid for the prediction of vertical wheel force for passenger vehicle. The algorithm pushes the area of vehicle transducerization application in road surface measurement into reality. It is suggested that future areas of study should examine the following:

1. Test other vehicle variants (light truck, commercial vehicle) and determine if this method continues to show good correlation to WFT.
2. Explore the application of nonlinear system identification, such as neural network, in force prediction.
3. Explore the correlation between angular acceleration and moment to predict 6DOF dynamic load.
4. Research on packaging the algorithm into microcomputer device for damage histogram data online monitoring.
5. Research the possibility of application in the field of active control by the algorithm.

References

1. Weiblen, W., Kockelmann, H., and Burkard, H., "Evaluation of Different Designs of Wheel Force Transducers (Part II)," SAE Technical Paper, SAE International 1999-01-1037, 1999, doi:10.4271/1999-01-1037.

2. Zhang, L., Liu, H., Zhang, H., and Xu, Y., "Component Load Predication from Wheel Force Transducer Measurements," SAE Technical Paper 2011-01-0737, 2011, doi:10.4271/2011-01-0737.
3. Cao, C., Ghosh, S., Rao, R., and Medepalli, S., "Truck Body Mount Load Prediction from Wheel Force Transducer Measurements," SAE Technical Paper 2005-01-1404, 2005, doi:10.4271/2005-01-1404.
4. Mathad, S.G., Chaturvedi, B., and Subramaniam, L., "An Integrated Approach to Extract Basic Suspension Data Through Integration of Tri-Axial Spindle Coupled Road Simulator, Wheel Force Transducer and a Wheel Vector Sensor," 2009.
5. Herrmann, M., Barz, D., Evers, W., and Barber, J., "An Evaluation of the Mechanical Properties of Wheel Force Sensors and their Impact on to the Data Collected during Different Driving Manoeuvres," SAE Technical Paper 2005-01-0857, 2005, doi:10.4271/2005-01-0857.
6. You, S.S., "Effect of Added Mass of Spindle Wheel Force Transducer on Vehicle Dynamic Response," SAE Technical Paper 2012-01-0210, 2012, doi:10.4271/2012-01-0210.
7. Meyer, R.A. and Sharp, M.C., "Optimizing Load Transducer Design Using Computer-Based Analytical Tools," SAE Technical Paper 2001-01-0787, 2001, doi:10.4271/2001-01-0787.
8. Sommerfeld, J.L. and Meyer, R.A., "Correlation and Accuracy of a Wheel Force Transducer as Developed and Tested on a Flat-Trac® Tire Test System," SAE Technical Paper 1999-01-0938, 1999, doi:10.4271/1999-01-0938.
9. Speckert, M., Ruf, N., Dressler, K. et al. , "Customer Usage Profiles, Strength Requirements and Test Schedules in Truck Engineering," Fraunhofer ITWM, 2010.
10. Ensor, D. and Cook, C., "Derivation of Durability Targets and Procedures Based on Real World Usage," *Technology* 2007, 2007, doi:10.4271/2007-26-074.
11. Dressler, K., Speckert, M., Müller, R., and Weber, C., "Customer Loads Correlation in Truck Engineering," *Berichte Des Fraunhofer ITWM* 151(151), 2009.
12. Andrew Halfpenny, M.P., "Proving Ground Optimization and Damage Correlation with Customer Usage," *SAE Int. J. Mater. Manuf.* 4(1):620-631, 2011, doi:10.4271/2011-01-0484.
13. Dobson, B.J. and Rider, E., "A Review of the Indirect Calculation of Excitation Forces from Measured Structural Response Data," *Proceedings of the Institution of Mechanical Engineers, Part C: Journal of Mechanical Engineering Science* 204(2):69-75, 1990, doi:10.1243/PIME_PROC_1990_204_080_02.
14. Cornelis, B., Risaliti, E., Tamarozzi, T., and Desmet, W., "Virtual Load Sensing Methods for Efficient Durability Testing and Customer Load Acquisition," *Dynamics (Pembroke, Ont.)* 8:9, 2016.
15. Ewins, D.J., "*Modal Testing: Theory and Practice*," (Letchworth, Research Studies Press, 1984).
16. Barber, A.J., "Accurate Models for Complex Vehicle Components Using Empirical Methods," SAE Technical Paper 2000-01-1625, 2000, doi:10.4271/2000-01-1625.
17. Pacejka, H., "*Tire and Vehicle Dynamics*," (Amsterdam, Elsevier, 2005).
18. Cochran, W.T., Cooley, J.W., Favin, D.L., Helms, H.D. et al., "What Is the Fast Fourier Transform?" *Proceedings of the IEEE* 55(10):1664-1674, 1967, doi:10.1109/PROC.1967.5957.
19. Johannesson, P. and Speckert, M., "*Guide to Load Analysis for Durability in Vehicle Engineering*," (John Wiley & Sons, 2013).
20. Vaughan, R., Temkin, M., and Lee, Y., "Criteria to Determine the Necessity of Data Acquisition for RTS Drive File Development Due to Vehicle Parameter Changes," *Automotive Engineering*, 2005, doi:10.4271/2005-01-0858.

Contact Information

The author can be contacted by email at: xushengjie@catarc.ac.cn or jayhsu0627@gmail.com.

Abbreviations

ASD - Auto Spectral Density
FEA - Finite Element Analysis
FFT - Fast Fourier Transform
FRF - Frequency Response Function
FWD - Front Wheel Drive
GVW - Gross Vehicle Weight
IFFT - Inverse Fast Fourier Transform
MIMO - Multiple Input Multiple Output
PG - Proving Ground
RDS - Related Damage Spectrum
RLD/RLDA - Road Load Data/ Road Load Data Acquisition
RMSE - Root Mean Square Error
WFT - Wheel Force Transducer
3DOF - Three Degree of freedom
6DOF - Six Degree of freedom

ISSN 0148-7191